




RESEARCH ARTICLE

Epileptic activity triggers rapid ROCK1-dependent astrocyte morphology changes

Stefanie Anders¹ | Björn Breithausen¹ | Petr Unichenko¹ | Michel K. Herde¹ |
 Daniel Minge¹ | Adlin Abramian¹ | Charlotte Behringer¹ | Tushar Deshpande¹ |
 Anne Boehlen¹ | Cátia Domingos¹ | Lukas Henning¹ | Julika Pitsch² |
 Young-Bum Kim³ | Peter Bedner¹  | Christian Steinhäuser¹  |
 Christian Henneberger^{1,4} 

¹Institute of Cellular Neurosciences, Medical Faculty, University of Bonn, Bonn, Germany

²Department of Epileptology, University Hospital Bonn, Bonn, Germany

³Division of Endocrinology, Diabetes, and Metabolism, Department of Medicine, Beth Israel Deaconess Medical Center, and Harvard Medical School, Boston, Massachusetts, USA

⁴German Center for Neurodegenerative Diseases (DZNE), Bonn, Germany

Correspondence

Christian Henneberger, Institute of Cellular Neurosciences, Medical Faculty, University of Bonn, Bonn, Germany.

Email: christian.henneberger@uni-bonn.de

Funding information

Deutsche Forschungsgemeinschaft, Grant/Award Numbers: SFB1089, SPP1757; National Institutes of Health, Grant/Award Number: R01DK129946; NRW-Rückkehrerprogramm; Human Frontiers Science Program

Abstract

Long-term modifications of astrocyte function and morphology are well known to occur in epilepsy. They are implicated in the development and manifestation of the disease, but the relevant mechanisms and their pathophysiological role are not firmly established. For instance, it is unclear how quickly the onset of epileptic activity triggers astrocyte morphology changes and what the relevant molecular signals are. We therefore used two-photon excitation fluorescence microscopy to monitor astrocyte morphology in parallel to the induction of epileptiform activity. We uncovered astrocyte morphology changes within 10–20 min under various experimental conditions in acute hippocampal slices. In vivo, induction of status epilepticus resulted in similarly altered astrocyte morphology within 30 min. Further analysis in vitro revealed a persistent volume reduction of peripheral astrocyte processes triggered by induction of epileptiform activity. In addition, an impaired diffusion within astrocytes and within the astrocyte network was observed, which most likely is a direct consequence of the astrocyte remodeling. These astrocyte morphology changes were prevented by inhibition of the Rho GTPase RhoA and of the Rho-associated kinase (ROCK). Selective deletion of ROCK1 but not ROCK2 from astrocytes also prevented the morphology change after induction of epileptiform activity and reduced epileptiform activity. Together these observations reveal that epileptic activity triggers a rapid ROCK1-dependent astrocyte morphology change, which is mechanistically linked to the strength of epileptiform activity. This suggests that astrocytic ROCK1 signaling is a maladaptive response of astrocytes to the onset of epileptic activity.

KEYWORDS

astrocytes, epilepsy, gap junction coupling, morphology, remodeling, ROCK signaling

Stefanie Anders, Björn Breithausen, and Petr Unichenko contributed equally to the study.

This is an open access article under the terms of the [Creative Commons Attribution](https://creativecommons.org/licenses/by/4.0/) License, which permits use, distribution and reproduction in any medium, provided the original work is properly cited.

© 2023 The Authors. GLIA published by Wiley Periodicals LLC.



1 | INTRODUCTION

Reactive astrogliosis is a cellular phenomenon that is found in many brain diseases including epilepsy. It describes the comprehensive morphological, biochemical, and functional transformation of astrocytes in parallel to the onset and progression of epilepsy (Escartin et al., 2021; Pekny & Pekna, 2014). The pathophysiological significance of such complex changes remains under debate. Studies show that reproducing features of astrocyte reactivity can lead to hyperexcitability of hippocampal networks (Ortinski et al., 2010) and spontaneous seizures (Robel et al., 2015). This indicates that reactive astrogliosis is a potential cause of epileptic activity and epilepsy and/or that it can sustain both. Therefore, understanding how reactive astrogliosis develops and identifying the involved molecular signals could be important for modifying the disease.

The interdependence of reactive gliosis and epilepsy and epileptogenesis has been intensely investigated in the hippocampus in the context of temporal lobe epilepsy, which is associated with a pronounced reactive astrogliosis. Like other brain regions, astrocyte morphology changes and the relationship to the onset or development of epilepsy are well documented in the hippocampus. These morphology changes are characterized by an increased expression of the glial fibrillary acidic protein (GFAP), which is an intermediate filament protein found in the larger main branches of astrocytes, cellular hypertrophy and an increase of larger GFAP-positive branches (Bordey & Sontheimer, 1998; Escartin et al., 2021; Niquet et al., 1994; Pekny & Pekna, 2014). In addition, several studies indicate that also smaller, perisynaptic astrocyte processes are remodeled in epilepsy or epilepsy models (Clarkson et al., 2020; Hawrylak et al., 1993; Witcher et al., 2010). Experimental models of temporal lobe epilepsy helped to establish the timeline of morphology changes. They revealed that astrocyte morphology changes can be detected at many time points like 2–4 weeks after induction of status epilepticus (Plata et al., 2018), 1 week after induction of focal epileptiform activity (Oberheim et al., 2008) and kainate-induced status epilepticus (Takahashi et al., 2010), and as early as 24–48 h after kindling using electrical stimulation (Hawrylak et al., 1993).

Interestingly, physiological changes of astrocyte morphology can also occur much faster on a time scale of minutes. Such fast dynamic repositioning of perisynaptic astrocyte processes around synapses over several minutes to up to half an hour has been observed in the hippocampus and elsewhere (Haber et al., 2006; Hirrlinger et al., 2004). In the hippocampus, induction of synaptic long-term potentiation can directly initiate this reconfiguration of perisynaptic astrocytic processes around synapses (Bernardinelli et al., 2014; Henneberger et al., 2020; Lushnikova et al., 2009). Because induction of synaptic plasticity usually leads to brief periods of increased network activity, we wondered if the onset of epileptic or epileptiform activity can trigger a similar process. This would change astrocyte morphology much faster than previously suggested.

We therefore performed two-photon excitation fluorescence microscopy for monitoring astrocyte morphology and its changes in the CA1 stratum radiatum of the hippocampus in acute slices. This was combined with electrophysiological experiments and induction of epileptiform activity. We indeed detected a robust change of smaller astrocyte processes in two in vitro epilepsy models, and in vivo after induction of status epilepticus. Preventing astrocyte remodeling in vitro revealed a role of astrocytic ROCK1 in both the astrocyte remodeling and the development of epileptiform activity.

2 | MATERIALS AND METHODS

2.1 | Experiments involving animals

All experiments involving animals were performed in full compliance with regulations of the European Union, the University of Bonn and the Landesamt für Natur, Umwelt und Verbraucherschutz (LANUV) North Rhine-Westphalia, Germany. Licenses for animal experiments were granted by the LANUV where needed (tamoxifen and kainate injections, see below). We used Wistar rats and mice of the following strains: mice expressing EGFP under a GFAP promoter (GFAP-EGFP, Nolte et al., 2001), GLASTcreERT2 (Mori et al., 2006), flox-stop-tdTomato (Madisen et al., 2010), ROCK1^{loxP/loxP} (Huang et al., 2012), ROCK2^{loxP/loxP} (Kümper et al., 2016), and TNF receptor 1 (TNFR1) knockout mice (Jackson Laboratory, #003242) (Peschon et al., 1998). GFAP-EGFP mice had an FVB background. GLASTcreERT2, flox-stop-tdTomato, ROCK1^{loxP/loxP} and ROCK2^{loxP/loxP} had an C57Bl/6N background. TNFR1 knockout mice had a C57Bl/6J background. To induce cre-dependent recombination, three-week-old mice were intraperitoneally injected with tamoxifen (100 mg/kg body weight) for 5 consecutive days (1 injection per day). In this case, recordings were performed 3–6 weeks after the first injection. Rats were used for experiments shown in Figures 1a–e, 3a, b, and 4. Mice were used in experiments shown in Figures 1f, g, 2, 3, 4c, d, 5, and 6. Their genotypes and further details are indicated in corresponding figures, text, and/or legends.

2.2 | Hippocampal slice preparation

Electrophysiology and two-photon excitation fluorescence microscopy in acute hippocampal slices were combined as previously described (Anders et al., 2014; Henneberger & Rusakov, 2012). Briefly, horizontal slices were obtained from 3- to 5-week-old Wistar rats (350 µm thick) and GFAP-EGFP mice (300 µm thick). Slices were prepared in an ice-cold slicing solution containing (in mM): NaCl 60, sucrose 105, KCl 2.5, MgCl₂ 7, NaH₂PO₄ 1.25, ascorbic acid 1.3, sodium pyruvate 3, NaHCO₃ 26, CaCl₂ 0.5, and glucose 10 (osmolarity 300–310 mOsm/L), and kept in the slicing solution at 34°C for 15 min before being stored at room temperature (21–23°C) in

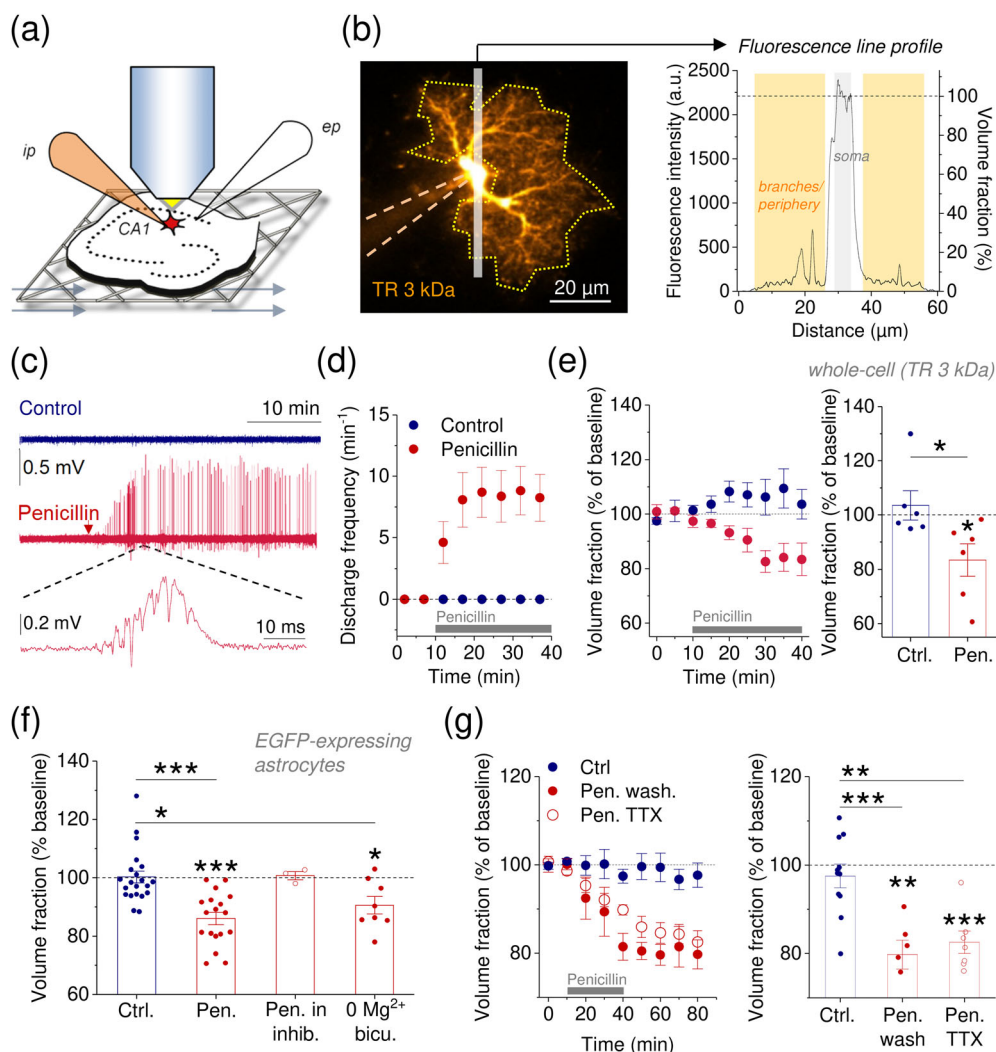


FIGURE 1 Induction of epileptiform activity rapidly alters astrocyte morphology in CA1 stratum radiatum. (a) Schematic recording configuration. Dye-filled (ip, intracellular pipette) or EGFP-expressing astrocytes in the CA1 stratum radiatum were visualized by two-photon excitation fluorescence imaging in parallel to monitoring of epileptiform activity (ep, extracellular pipette) in acute hippocampal slices resting on a grid to allow perfusion from both sides. (b) Sample focal section through the soma of an astrocyte filled with Texas Red Dextran 3 kDa (300 μ M, TR 3 kDa) via the whole-cell patch pipette (left panel, dotted lines). A fluorescence intensity line profile (right panel) taken through the soma (position of line profile indicated by bar in left panel) shows the characteristic fluorescence distribution throughout the periphery of the cell and the soma (100% of the tissue is occupied by the astrocyte at its soma). The fraction of tissue volume occupied by the astrocyte (astrocyte volume fraction) was calculated by normalizing the average fluorescence intensity of the periphery (left panel, dotted polygonal region) to the somatic fluorescence intensity. (c) Sample electrophysiological control recording (control, blue, top trace) and recording with induction of epileptiform activity by bath application of penicillin (penicillin, red, middle trace) after a 10-min baseline period (start indicator by arrow). Zoomed-in section with epileptiform discharge in lower panel. (d) Penicillin reliably induced stable epileptiform discharges, which were not observed in control recordings. (e) Left panel: Time course of the astrocyte volume fraction in control recordings (blue, $n = 6$) and during induction of epileptiform activity (red, $n = 6$). Right panel: The volume fractions at the end of the experiment were significantly lower when epileptiform activity had been induced ($p = .031$, unpaired Student's t -test vs. control, one population Student's t -test vs. 100%, $p = .54$ for control and $p = .038$ for penicillin). (f) Equivalent experiments were performed on mouse hippocampal slices with astrocytes expressing EGFP (Nolte et al., 2001). Analysis of volume fraction changes at the end of the experiments (10 min baseline and 30 min of further recording). No change under control conditions (Ctrl., $100.2 \pm 2.04\%$, $n = 21$, $p = .91$, one population Student's t -test). Induction of epileptiform activity decreased the astrocyte volume fraction to $86.0 \pm 2.13\%$ (penicillin, Pen., $n = 18$, $p < .001$, one population Student's t -test). This effect was absent in the presence of the channel/receptor inhibitors TTX (1 μ M), NBQX (10 μ M) and D-APV (50 μ M) (Pen. in inhib., $100.7 \pm 1.39\%$, $n = 3$, $p = .66$, one population Student's t -test). Similar reduction of the volume fraction after induction of epileptiform activity by bath application of bicuculline (50 μ M, $90.6 \pm 2.99\%$, $n = 8$, $p = .016$, one population Student's t -test) in the absence of extracellular Mg^{2+} (0 Mg^{2+} bicuculline). Comparisons by unpaired Student's tests: penicillin versus control $p < .001$, 0 Mg^{2+} and bicuculline versus control $p = .016$. (g) Left panel: Time course of experiments with washout of penicillin after 40 min (filled red circles, Pen. wash.), wash-in of TTX after 40 min (hollow red circles, Pen. TTX), and control experiments (filled blue circles, Ctrl.). EGFP-expressing astrocytes. Right panel: Statistics of volume fraction changes at the end of the experiment (one populations Student's t -test vs. 100%: Ctrl. $p = .38$, $n = 11$; Pen. wash $p = .0017$, $n = 6$; Pen. TTX $p < .001$, $n = 7$). Astrocyte volume fraction reductions persisted after wash-out of penicillin and wash-in of TTX (two populations Student's t -tests: Ctrl. vs. Pen. wash $p < .001$, Ctrl. vs. Pen. TTX $p = .00149$).

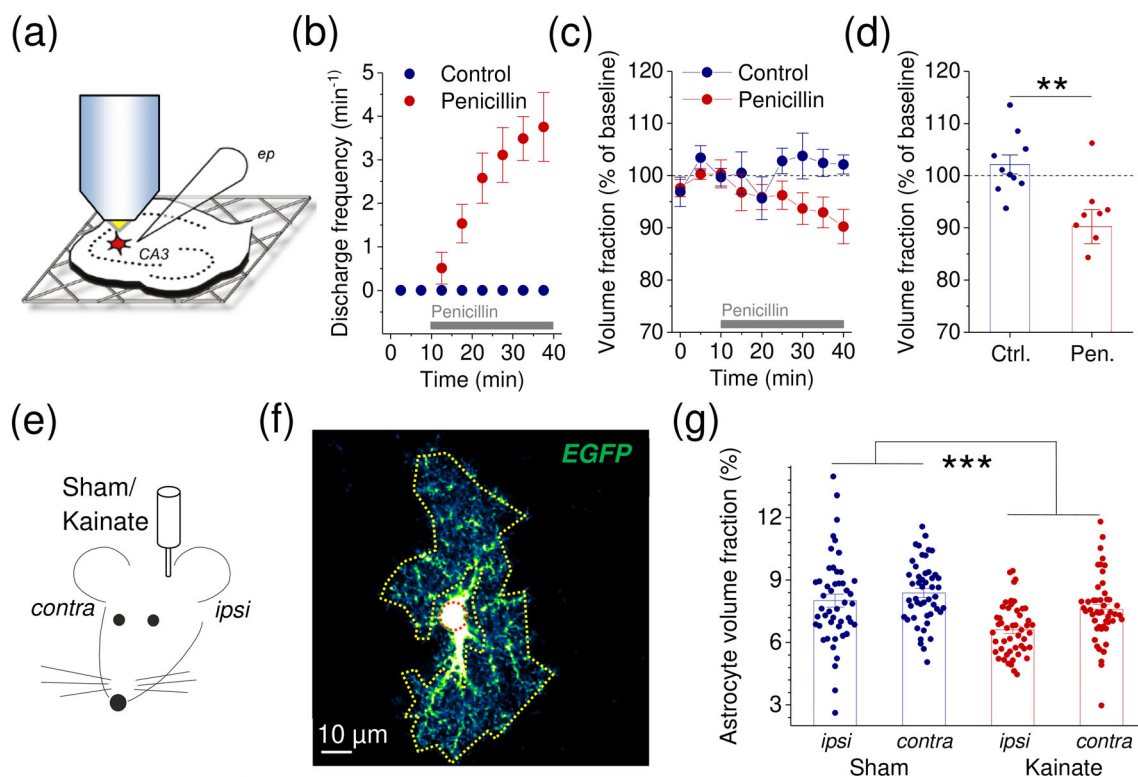


FIGURE 2 Rapid astrocyte morphology changes in CA3 stratum radiatum in vitro and in CA1 stratum radiatum in vivo. (a) The volume fraction of EGFP-expressing astrocytes in CA3 stratum radiatum and field potentials was monitored. (b) Acute bath application of penicillin reliably induced epileptiform discharges ($n = 8$, red dots), which were absent in control recordings ($n = 10$, blue dots). (c) Emergence of epileptiform activity was accompanied by a reduction of the astrocyte volume fraction (red), which was not observed in control recordings (blue). Number of experiments and animals as in (b). (d) Comparison of astrocyte volume fractions relative to baseline at the end of the experiment (Student's unpaired t -test, $p = .0050$). Number of experiments and animals as in (b). (e) Schematic illustration of the in vivo experiment. Kainate (70 nL, 20 mM) was injected immediately above the right dorsal hippocampus to induce status epilepticus in three mice expressing EGFP in astrocytes. Saline sham injections were performed in another three mice. Perfusion fixation of animals 30 min after injection. (f) Single focal section of an astrocyte in the CA1 stratum radiatum (focal plane through soma). The astrocyte volume fraction was analyzed by normalizing the average territory fluorescence (yellow dotted region) to the somatic fluorescence (red dotted circle). (g) Blinded analysis of volume fractions of astrocytes from the ipsilateral and contralateral hippocampus after sham/kainate injection ($n = 48, 49, 49$, and 49 astrocytes from left to right from three independent experiments in each group). Two-way ANOVA indicated a significant effect of the site ($p = .0046$) and treatment ($p < .001$, indicated by asterisks) but no significant interaction of the two factors (treatment and site, $p = .20$).

an artificial cerebral spinal fluid (ACSF) containing (in mM): NaCl 131, KCl 2.5, MgSO_4 1.3, CaCl_2 2, NaH_2PO_4 1.25, NaHCO_3 21, and glucose 10 (osmolality adjusted to 295–305 mOsm/L). Slices were allowed to rest for at least 60 min. For recordings, slices were transferred to a double-perfusion submersion-type recording chamber and perfused with extracellular solution (ACSF). All recordings were performed at 33–35°C. All solutions were continuously bubbled with 95% O_2 /5% CO_2 .

2.3 | Electrophysiology

Extracellular recordings were performed using patch pipettes filled with extracellular solution. Whole-cell recordings from neurons and astrocytes were obtained using standard patch pipettes (3–4 M Ω) filled with an intracellular solution containing (in mM): $\text{KCH}_3\text{O}_3\text{S}$ 135, HEPES 10, di-tris-phosphocreatine 10, MgCl_2

4, $\text{Na}_2\text{-ATP}$ 4, Na-GTP 0.4 (pH adjusted to 7.2, osmolality 290–295 mOsm/L). Membrane-impermeable dyes were added to the intracellular solution as indicated: Texas Red dextran 3 kDa (300 μM) to capture astrocyte morphology changes, Alexa Fluor 594 hydrazide (40 μM , Invitrogen) for astrocyte coupling experiments. Astrocytes were identified using infrared differential interference contrast or Dodt contrast optics by their small soma size ($\sim 10 \mu\text{m}$), low resting potential ($< -80 \text{ mV}$ without correction for the liquid-junction potential), low input resistance ($< 10 \text{ M}\Omega$, current clamp), passive (ohmic) whole-cell current patterns, characteristic morphology, and dye coupling (visualized in the Alexa emission channel). Astrocytes were either held in voltage clamp mode at their resting membrane potential or in current clamp. Evoked GABAergic inhibitory postsynaptic currents (eIPSCs) were recorded in presence of APV and NBQX from visually identified CA1 pyramidal cells held at -70 mV in voltage clamp. In these experiments extracellular KCl concentration was elevated to 4 mM

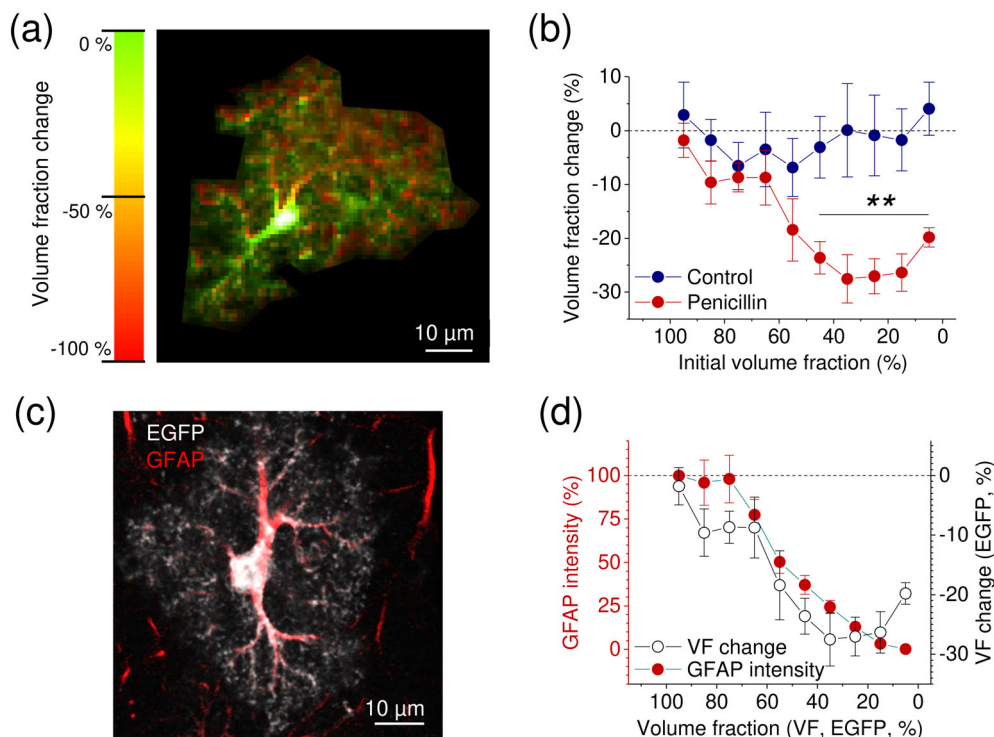


FIGURE 3 Peripheral volume reduction of mostly glial fibrillary acidic protein (GFAP)-negative astrocyte processes after induction of epileptiform activity. (a) Volume fraction changes were mapped onto astrocyte territories (color encodes change according to scale, brightness encodes initial volume fraction). Note the volume fraction reduction (reddish colors) in the periphery of this example from an experiment with induction of epileptiform activity. (b) Relationship between initial volume fraction and volume fraction reduction from control recordings and recordings with induction of epileptiform activity. Significant volume fraction changes in the territory of astrocytes occur where the initial volume fraction was low (two-way repeated measure ANOVA $p < .001$, post hoc Fisher pairwise comparisons $p < .01$ as indicated, $n = 10$ and 12 for control and penicillin respectively), that is, in the parts of the focal plane dominated by small astrocyte processes. (c) For obtaining further information about the observed rapid morphology change, we investigated the relationship between the volume fraction (VF) of local astrocyte processes (EGFP-expressing) and their GFAP expression using immunohistochemistry (see Methods). Note the strong GFAP signal in bigger main processes. (d) Relationship between local astrocyte VF and GFAP intensity ($n = 10$ astrocytes from two independent experiments). For comparison, the dependence of the VF change after epileptiform activity on the initial VF from (b) is replotted (hollow circles). The local VF change is strongly correlated with the local GFAP-intensity (Spearman $R = 0.818$, $p = .0038$): The lower the GFAP-intensity the more negative the VF change, that is, the stronger the local VF reduction.

and QX314 (5 mM) was added to an intracellular solution containing (in mM): KCl 135, HEPES 10, di-Tris-Phosphocreatine 10, $MgCl_2$ 2, Na_2 -ATP 4, Na -GTP 0.4 (pH adjusted to 7.2, osmolarity 290–295 mOsm/L). Data were recorded using MultiClamp 700B (Molecular Devices) and EXT-02B (npi Germany) amplifiers, digitized (10–40 kHz) and stored for offline analysis. Whole-cell patch clamp recordings were rejected if at any time the access resistance exceeded 20 M Ω or changed by more than 20%. Bridge balance and series resistance compensation was used as appropriate. For stimulation experiments, a bipolar concentric stimulation electrode was placed in the stratum radiatum at the border between CA2/3 and CA1. Stimulation intensities (DS3, Digitimer Ltd., UK) were set to obtain ~50% of the maximum fiber volley amplitude.

Epileptiform activity was induced by bath application of 4 mM penicillin G sodium salt for 30 min. Spontaneous epileptiform discharges were recorded in CA1 stratum pyramidale in rat and mouse hippocampal slices. After 10–20 min of baseline recording, slices were recorded under either control or penicillin conditions. The

extracellular K^+ concentration throughout the experiment was 5 mM when acute slices from rats were used and 4 mM for acute slices from mice. To examine the persistence of epileptiform activity penicillin was washed out after 30 min of application for another 40–50 min. Spontaneous epileptiform discharges were recorded throughout the experiment.

In some experiments, the inhibitors D-AP5 (APV in text and figures, 50 μ M, Abcam), NBQX disodium salt (10 μ M, Abcam), CGP52432 (5 μ M, Abcam) and tetrodotoxin (TTX, 1 μ M, Tocris), rhosin, (30 μ M, Tocris), NSC 23766 (100 μ M, Tocris), and Y-27632 (5 μ M, Tocris) were added to the extracellular solution as indicated.

2.4 | Two-photon excitation fluorescence microscopy

Astrocytes and their gap junction-coupled networks were visualized by two-photon excitation fluorescence microscopy. We used a

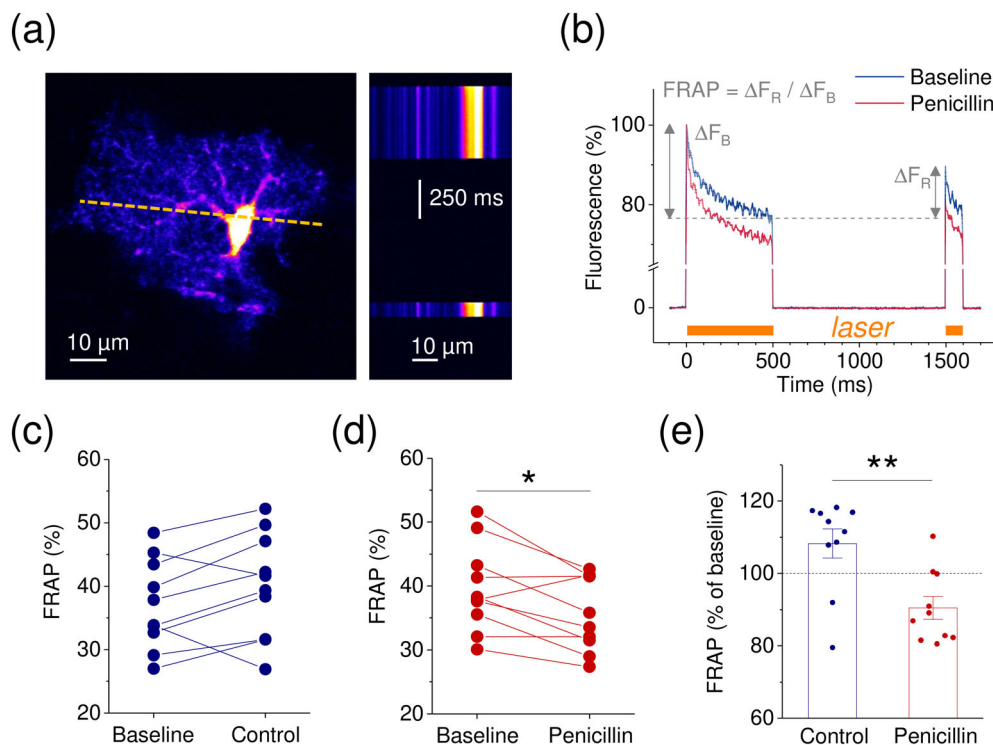


FIGURE 4 Induction of epileptiform activity decreases intracellular diffusion in astrocytes. (a) Intracellular diffusion within astrocytes was quantified by fluorescence recovery after photobleaching (FRAP) of EGFP expressed by astrocytes and was used to gauge intracellular diffusivity. Bleaching was induced by high power scanning (right panel) along a line crossing the astrocyte territory (dashed line in left panel). Fluorescence recovery occurred when unbleached EGFP diffused into the imaged region while the laser shutter was closed for 1 s (right panel). (b) Quantification of (a) (orange bars indicate laser exposure). The bleached fraction of fluorescence ΔF_B and the recovered fraction ΔF_R were measured and used to quantify $FRAP = \Delta F_R / \Delta F_B$. (c, d) FRAP was recorded at the beginning (Baseline) and the end of individual experiments (Control/Penicillin for 30 min). In control recordings, a slight but statistically insignificant increase was observed (e, $p = .074$, $n = 10$, paired t -test). In contrast, induction of epileptiform activity reduced FRAP significantly (f, $p = .016$, $n = 10$, paired t -test). (g) FRAP relative to baseline was significantly lower when epileptiform activity had been induced ($p = .0027$, $n = 10$ both groups, unpaired t -test).

Scientifica two-photon system (Scientifica, UK) and a FV10MP imaging system (Olympus) optically linked to a femtosecond pulse laser Vision S (Coherent, excitation $\lambda = 800$ nm) both integrated with patch-clamp electrophysiology. For imaging of tdTomato fluorescence, the excitation wavelength was set to 915 nm. Setups were equipped with $25\times$ (NA 1.05) and $40\times$ (NA 0.8) objectives (Olympus). The laser power was adjusted for recording depth to obtain fluorescence intensities equivalent to those recorded from the slice surface with 2–3 mW under the objective.

EGFP-expressing and Texas Red Dextran 3 kDa filled astrocytes were used for monitoring astrocyte morphology in parallel to induction of epileptiform activity as indicated. In experiments with astrocytes dye-loaded via the whole-cell patch clamp pipette, Texas Red Dextran 3 kDa typically equilibrated across the astrocyte arbor within 10–15 min. Shallow image stacks containing the astrocyte soma (512×512 pixels, $0.1 \times 0.1 \mu m^2$ per pixel, 3 slices [each an average of three frames], $1 \mu m$ z-spacing) were obtained every 5–10 min. For analysis of the astrocyte volume fraction (VF) (Henneberger et al., 2020; Medvedev et al., 2014; Minge et al., 2021) an initial focal plane passing through the soma was chosen. In subsequent stacks, the focal plane closest to the initial one was chosen for analysis. For a

VF time series, an initial region of interest covering the entire astrocyte territory except the soma (see Figure 1b for illustration) and a somatic region of interest were defined and the background-corrected fluorescence intensities F and F_{SOMA} were determined for each time point. The VF time series was calculated for each time point by $VF = F/F_{SOMA}$.

The strength of astrocyte coupling was determined as previously described (Anders et al., 2014). Briefly, two additional image stacks were acquired after 20 min of dye loading (512×512 pixels, $<0.7 \mu m/pixel$, stack size $>200 \times 200 \times 80 \mu m^3$) and at the end of a penicillin application or control recording. Gap junction-coupled cells were manually identified in x-y-z image stacks and their somatic (region of interest $5 \times 5 \mu m^2$) background-corrected fluorescence intensities were determined and corrected for depth in the tissue. The three-dimensional distances of dye-coupled cells were calculated relative to the patched cell. The relationship between distance and relative fluorescence intensity was fitted by a monoexponentially decaying function to obtain the coupling length constant (Figure 5).

To map VF changes of EGFP-expressing astrocytes onto the initial VF distribution (Figure 3a, b), background-corrected images of the same astrocyte at the beginning and at the end of a recording were

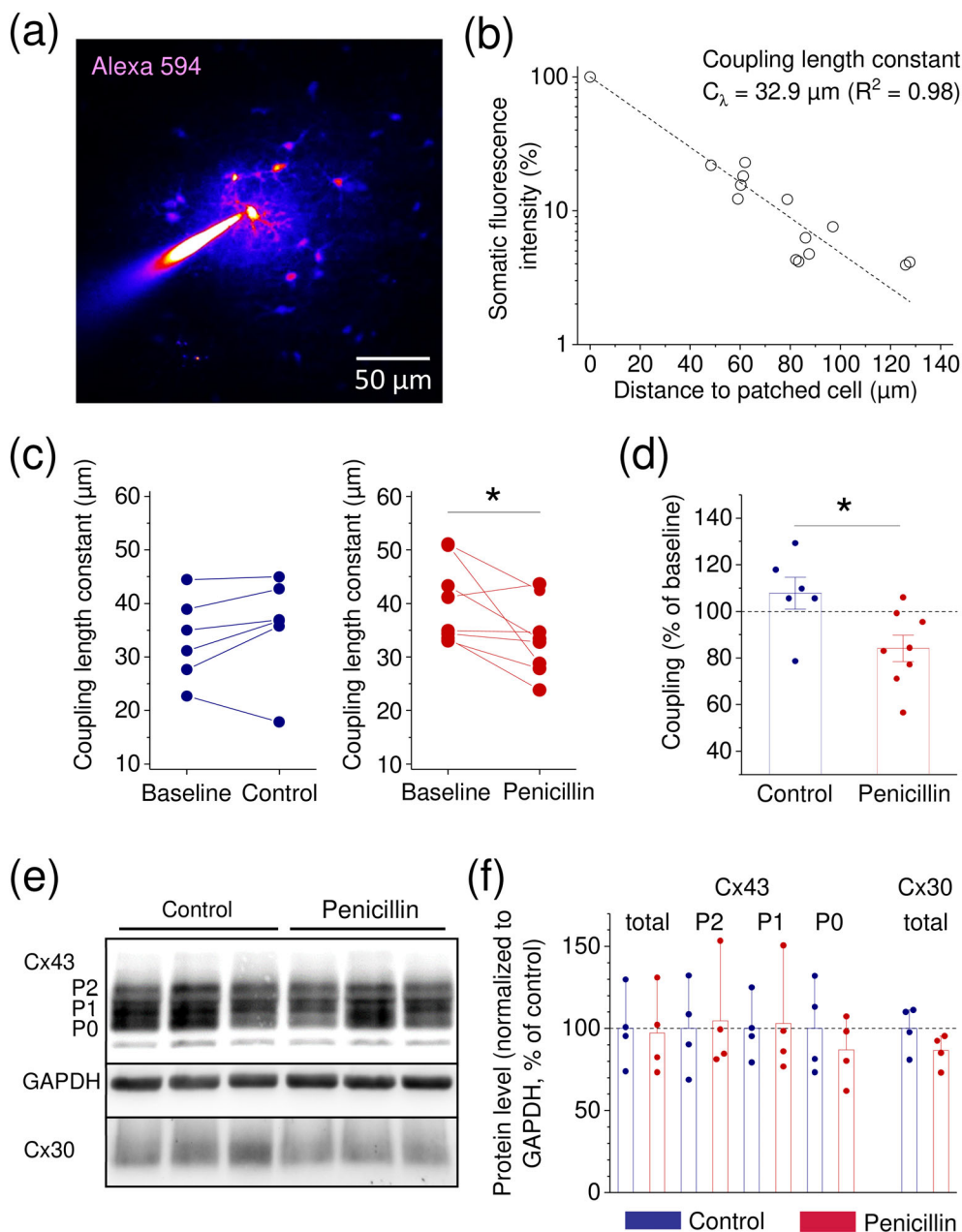


FIGURE 5 Reduced astrocyte gap junction coupling after induction of epileptiform activity. (a) Astrocytes were loaded with Alexa 594 hydrazide (40 μM) via the whole-cell patch pipette. x-y-z stacks were obtained after 20 min of loading (Baseline) and at the end of the experiment (30 min after wash-in of penicillin, Penicillin, or 30 min of control conditions, Control). A sample z-projection of a loaded astrocyte network and the patch pipette is shown. Note the bright fluorescence of the patched cell and the decaying intensity of coupled cells with increasing distance. (b) The coupling length constant as a measure of coupling strength was obtained by a monoexponential fit of the fluorescence intensity relative to the patched cell and the distance to the patched cell (Anders et al., 2014). (c) No significant change in control recordings from 20 (Baseline) to 50 min (Control, left panel, $p = .229$, $n = 6$, paired Student's t -test). In contrast, induction of epileptiform activity reduced the coupling length constant (right panel, $p = .040$, $n = 8$, paired Student's t -test). (d) While the baseline coupling length constants were not different between experimental groups ($p = .120$, $n = 6$ and 8 , unpaired Student's t -test, not illustrated), the coupling constant after 50 min, relative to baseline values, was significantly lower after induction of epileptiform activity ($p = .020$, $n = 6$ and 8 , unpaired Student's t -test). The whole-cell access resistances did not differ between groups ($p > .4$, unpaired Student's t -tests). (e) Connexin 43 (Cx43) and 30 (Cx30) expression and Cx43 phosphorylation was analyzed in acute slices after control experiments and after induction of epileptiform activity. Representative immunoblots showing Cx43, GAPDH (control) and Cx30. Cx43 shows a characteristic 3 band pattern (P2, P1, and P0) representing different phospho-isoforms while Cx30 shows a single band. (f) Band intensities normalized to corresponding GAPDH intensities and expressed as a percentage of the mean of the control group. No significant difference between control and penicillin groups for total Cx43 and Cx30 protein levels. The levels of phospho-isoforms were also comparable between the groups ($p > .4$ throughout, unpaired Student's t -test, $n = 4$ independent experiments in each group, 5–6 acute slices per independent experiment).

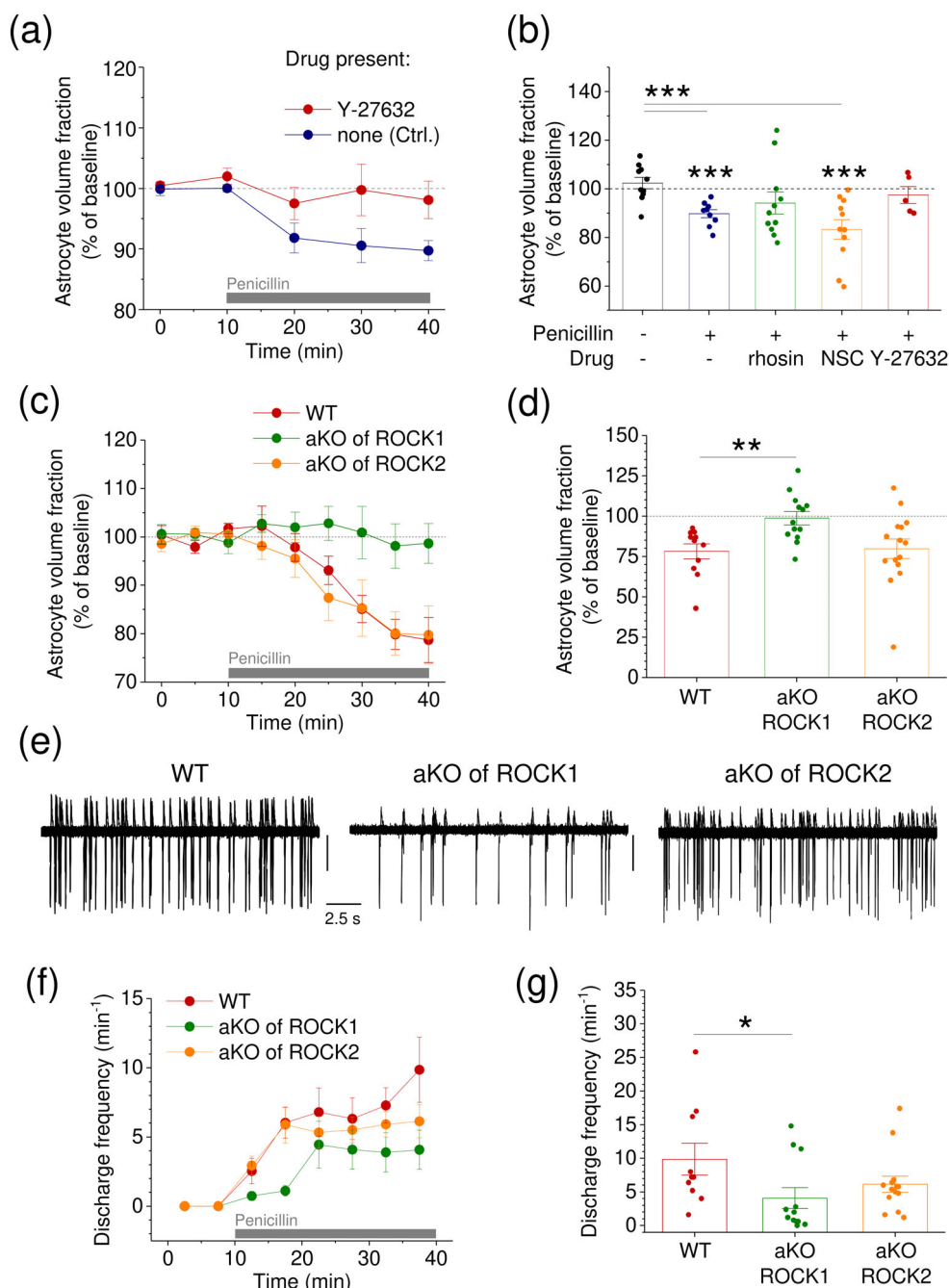


FIGURE 6 Astrocytic ROCK signaling drives astrocyte morphology changes and supports epileptiform activity. (a) Examples of pharmacological experiments on astrocyte volume fraction changes. The volume fraction of EGFP-expressing astrocytes was monitored during the induction of epileptiform activity using penicillin. A drug was either present (here Y-27632, 5 μM , red, $n = 5$) in the bath solution throughout the experiment or not (Ctrl., blue, $n = 10$). (b) Summary of pharmacological experiments on volume fraction changes. Drugs and penicillin application are indicated below the x-axis (RhoA inhibitor rhosin, 30 μM , Rac1 inhibitor NSC 23766, 100 μM , ROCK inhibitor Y-27632, 5 μM). One population Student's t -test versus 100% from left to right: $p = .34$, $n = 10$; $p < .001$, $n = 9$; $p = .23$, $n = 11$, $p = .0020$, $n = 11$; $p = .51$, $n = 5$. Two populations Student's t -tests versus no drug and no penicillin: penicillin no drug present $p < .001$, penicillin NSC 23766 present $p < .001$, all other $p > .10$. (c) Comparison of slice experiments from ROCK1/2 wildtype (WT), astrocytic knockout (aKO) of ROCK1 and aKO of ROCK2 mice (see text for details). Astrocytes expressed tdTomato in these experiments to monitor their volume fraction changes ($n = 11$ WT, $n = 13$ aKO of ROCK1, $n = 15$ aKO of ROCK2). (d) Comparison of volume fractions after 40 min. Mann-Whitney U-tests: WT versus aKO of ROCK1 $p = .0054$, WT versus aKO of ROCK2 $p = .69$. (e) Example of epileptiform activity induced by penicillin in all three conditions (vertical scale bars 0.4 mV, 20 superimposed traces for each condition). (f) Development of epileptiform activity during penicillin application (indicated by gray bar). (g) Comparison of epileptiform discharge frequency after 40 min. Mann-Whitney U-tests: WT versus aKO of ROCK1 $p = .019$, WT versus aKO of ROCK2 $p = .12$.

compared. Both images were shrunk by a factor of 10 by averaging regions of 10×10 pixels (i.e., $1 \times 1 \mu\text{m}^2$) and their fluorescence intensities were normalized to somatic values to obtain a VF map of both images. For each pixel within the territory of the cell, the initial VF and its change were calculated, and color coded as displayed (Figure 3a). VF changes were correlated with the initial VF by calculating mean changes over initial VF ranges (0%–10%, 10%–20%, ... 90%–100%).

Throughout the analyses described above, the astrocyte territories and regions of interests were determined manually by visual inspection. For recordings in which astrocytes were repeatedly imaged, the astrocyte territories and regions of interest were set based on the first baseline recording and kept constant for subsequently recorded images from the same experiment. Changes relative to baseline, for instance of the VF, were used throughout to minimize potential biases introduced by manual setting of territories and regions of interest. In experiments in which absolute VFs were compared (experiments with status epilepticus, see below), analysis was performed fully blinded and individual data points and experimental groups were only revealed after complete analysis. In analyses in which changes of the astrocyte cross-section area were quantified, we measured the area of the cross section of the astrocytes from the first and last recorded image by drawing polygonal regions of interest around the astrocytes and calculating their areas. No blinding was performed for the latter analysis.

Fluorescence recovery after photobleaching (FRAP) of EGFP was used to gauge intracellular diffusivity as previously described (Anders et al., 2014; Henneberger et al., 2020). Briefly, FRAP was measured by line scanning across astrocyte cross-sections (Figure 4a, b) at 1–3 ms/line and using the following protocol during the scan: (1) Bleaching was induced by scanning with the laser power at the objective set to 15–30 mW for the initial 500 ms. The laser shutter was then closed for 1 s, which allows unbleached EGFP to diffuse into the scanned tissue, that is, for the EGFP fluorescence to recover. Scanning is then continued for 100 ms at the increased laser power (typical fluorescence profile in Figure 4a). The background-corrected fluorescence over time is then normalized to the initial value (Figure 4b). After that, FRAP is quantified by first calculating the fraction of bleached EGFP (ΔF_B) and the fraction of recovered EGFP fluorescence (ΔF_R), which is a measure of the amount of unbleached EGFP that diffused into the scanned tissue when the laser shutter was closed. The ratio ($\Delta F_R/\Delta F_B$) was used as a measure of FRAP. See (Anders et al., 2014) and supplementary material therein for further information. Two FRAP experiments were performed during recordings. One during the baseline period and one at the end of the experiment (30 min of penicillin application or 30 min of control recording).

2.5 | In vivo kainate injection

In vivo kainate injections were used to induce status epilepticus in mice expressing EGFP in astrocytes as previously described (Bedner et al., 2015). Briefly, three-months-old mice were anesthetized with a mixture of medetomidine (Cepetor, 0.3 mg/kg, i.p., CP-Pharma) and

ketamine (Ketamidol, 40 mg/kg, i.p., WDT) and placed in a stereotaxic frame equipped with a manual microinjection unit (TSE Systems GmbH). 70 nL of a 20 mM solution of kainate (Tocris) in 0.9% sterile NaCl were stereotactically injected into the cortex just above the right dorsal hippocampus using a 0.5 μL microsyringe (Hamilton). The stereotactic coordinates were 1.9 mm posterior to bregma, 1.5 mm from midline and 1.7 mm from the skull surface. Control mice were given injections of 70 nL saline under the same conditions. 30 min after injection, deep anesthesia was ensured by injecting a mixture of 225 mg/kg ketamine and 15 mg/kg xylazine (Sigma-Aldrich). Then mice were immediately transcardially perfused with ice-cold 4% paraformaldehyde in phosphate buffered saline (PBS, pH 7.4). The brains were gently removed from the skull and postfixed in 4% paraformaldehyde (in PBS) at 4°C for 12 h. 40 μm -thick coronal sections of the dorsal hippocampus were cut on a vibratome (Leica) and washed for 3×10 min in PBS before being mounted and coverslipped using ProLong Antifade Diamond (Invitrogen). Image stacks of EGFP fluorescence of CA1 stratum radiatum astrocytes ($n = 15$ – 18 per hemisphere per animal, from slices within or immediately adjacent to the kainate injection site) were obtained on a Leica SP8 confocal microscope using a $63\times/1.2\text{NA}$ water immersion objective. Image planes through the center of the soma were extracted from the image stacks and analyzed independently by experimenters blinded to the experimental condition to obtain the astrocyte VF (see above).

2.6 | Immunohistochemistry

For correlating the local astrocyte VF and the local (subcellular) GFAP expression, we performed GFAP-immunohistochemistry on sections of CA1 stratum radiatum with EGFP-expressing astrocytes (GFAP-EGFP, Nolte et al., 2001). Briefly, six-week-old GFAP-EGFP mice were deeply anesthetized by intraperitoneal injection of a ketamine/xylazine solution and transcardially perfused with ice-cold 4% PFA in PBS. Their brains were then removed and postfixed in PFA at 4°C overnight. Coronal brain sections of (70 μm thickness) were cut on a vibratome (Leica, VT1200S; Leica Microsystem) and washed $3 \times$ for 10 min in PBS. Slices selected for immunostaining were then incubated in a permeabilization and unspecific binding block solution (0.5% Triton X-100, 5% normal goat serum in PBS) for 1–1.5 h at room temperature (RT). Afterwards, brain slices were incubated with the primary antibodies chicken anti-GFP (1:500, Abcam, ab13970) and mouse anti-GFAP (1:500, Millipore, MAB360) diluted in PBS at 4°C overnight. After 3×10 min washing in PBS at RT, slices were incubated with the secondary antibodies goat anti-chicken Alexa Fluor 488 (1:500, Invitrogen, A11039) and biotin-SP-AffiniPure Fab fragment goat anti-mouse (1:500, Jackson ImmunoResearch, 115-067-003) diluted in PBS for 2–2.5 h at RT. GFAP was visualized using the biotin-labeled secondary antibody and a third incubation step with Alexa Fluor 647 conjugated streptavidin (1:200, Johnson ImmunoResearch, 016-600-084). Finally, slices were washed $3 \times$ for 10 min in PBS and mounted with Invitrogen



Prolong Diamond Antifade mountant (P36965) and left for curing for at least 24 h at 4°C.

For analysis, confocal fluorescence microscopy of EGFP-expressing astrocytes and the corresponding GFAP label was performed (1024 × 1024 pixels, 96 μm × 96 μm) using a Leica SP8 confocal microscope with a 40×/1.1 NA objective. For each astrocyte, both images (i.e., EGFP and GFAP) were background-corrected and shrunk by a factor of ~10 by averaging regions of 1 × 1 μm², as above. For EGFP images, their fluorescence intensities were normalized to somatic values to obtain a map of the astrocyte VF. For each pixel within the territory astrocyte, the VF and the corresponding GFAP label intensity were calculated. GFAP intensities were correlated with the local astrocyte VF by calculating their average over VF ranges (0%–10%, 10%–20%, ... 90%–100%). For each analyzed cell, these mean GFAP intensities were normalized to somatic values to account for variable staining efficacies between experiments. Then, we calculated the average dependence of the GFAP intensity on the local astrocyte VF (Figure 3d).

2.7 | Western blots

Western blot analysis of connexin (Cx) expression and phosphorylation was performed on acute hippocampal slices after control recordings or after induction of epileptiform activity using penicillin. Hippocampi were cut out from acute slices and quickly frozen in liquid nitrogen for 5 min followed by storage in –80°C until further use. 5–6 slices were pooled for individual experiments to obtain enough protein for western blotting. Samples were homogenized in ice-cold 50 mM Tris buffer (pH 7.4) containing 150 mM NaCl, 1% Triton-X 100, 0.5% NP-40, and 0.5% sodium deoxycholate. Lysates were sonicated, passed through 30-gauge syringes to shear DNA and centrifuged at 1000 g for 5 min. The protein concentrations of supernatants were measured (BCA assay, ThermoFisher) and 30 μg of protein were subjected to SDS PAGE (12.5%) followed by western blotting on polyvinylidene difluoride membranes (Millipore). The membranes were blocked with 5% non-fat dry milk in tris-buffered saline with Tween-20 (TBST) for 1 h followed by overnight incubations in primary antibody solutions prepared in 2.5% non-fat dry milk in TBST. All incubations were followed by 3 times washes in TBST. The following primary antibodies were used: custom-made rabbit anti-Cx43 directed against amino acid residues 360–382 at 1:2500 (Deshpande et al., 2017), mouse anti-GAPDH (Abcam, 1:5000) and rabbit anti-Cx30 (ThermoFisher, 1:250). Membranes were probed with goat anti-mouse horseradish peroxidase conjugate and goat anti-rabbit horseradish peroxidase conjugate antibodies (both 1:10,000, GE Healthcare). Peroxidase activity was visualized using WesternBright Sirius™ substrate (Advansta) and detected using Gene Gnome (Synoptics). Images were taken using a gel photography system with 16bit resolution. Care was taken to avoid image saturation (highest intensity throughout of 15,698). Expression levels were quantified using Gene Tools quantification software (Synoptics) with GAPDH intensity as a reference.

2.8 | K⁺-sensitive microelectrode recordings

K⁺-sensitive microelectrodes were prepared as previously described (Breithausen et al., 2020). Briefly, theta borosilicate glass capillaries (Hilgenberg GmbH, Germany) were pulled to a tip diameter of 1–2 μm. The reference barrel was filled with 154 mM NaCl solution, the K⁺-sensitive barrel was filled with 100 mM KCl, after the tip of the K⁺-sensitive barrel had been silanized by a mixture (20:1) of dichloromethane (Sigma-Aldrich) and trimethylchlorosilane (Sigma-Aldrich). The tip of the K⁺-sensitive barrel was then filled with a valinomycin-based K⁺-exchanger solution (potassium ionophore I cocktail A, Sigma). Chloride coated silver-wires (Science Products, Germany; diameter: 200 μm) were inserted into both barrels and fixed with hard wax. Recordings were performed using a differential amplifier (ION-01 M, npi, Germany). Electrodes were calibrated with solutions containing 3 mM and 30 mM KCl in 154 mM NaCl and displayed voltage responses of $s = 57.8 \pm 0.45$ mV ($n = 7$) per 10-fold increase of $[K^+]_O$. The recorded voltage signal recorded was converted to a K⁺ concentration using $[K^+]_O = (10^{(E/s)} \times [K^+]_B)$, where E is the measured potential and $[K^+]_B$ is the nominal resting potassium concentration, that is, the potassium concentration of the extracellular solution. K⁺-transients were recorded from the CA1 stratum radiatum and evoked by a high-frequency stimulus (50 pulses at 100 Hz, repeated 10 times at an interval of 60 s) in the presence of the glutamate receptor blockers (D-AP5, 50 μM, and NBQX, 10 μM). A second field recording pipette in the CA1 stratum pyramidale was used to monitor epileptic discharges, field responses and fiber volleys. Responses were normalized to the corresponding mean fiber-volley amplitude to account for differences in stimulation efficiency between slices and preparations. Fiber volley amplitudes for normalization were recorded with the reference barrel of the K⁺-sensitive microelectrodes.

2.9 | Analysis and statistics

Analyses were performed using ImageJ (NIH), Origin (OriginLab) and Matlab (MathWorks). Numerical data are reported as mean ± SEM with n being the number of samples. In all electrophysiological and imaging experiments in acute hippocampal slices, n refers to the number of recordings. One recording was performed per acute hippocampal slice. Because the success rate of experiments combining electrophysiology, two-photon excitation imaging and pharmacology is low, a single successful experiment was typically performed per day and animal. For all other experimental designs (Figures 2e–g, 3c, d, and 5e, f) detailed information can be found in the figure legends. The Shapiro–Wilk test was used to establish if data were normally distributed. Comparisons were then performed using the appropriate parametric and non-parametric tests (e.g., Student's t -test or Mann–Whitney U-test). The statistical tests used are indicated throughout. In figures, asterisks indicate significance levels where *** $p < .001$, ** $p < .01$, and * $p < .05$, and error bars represent SEM in figures and dots

represent individual data points. Asterisks immediately above bars in bar plots refer to single population tests against a reference (details in the figure legend). Asterisks above lines connecting bars in bar plots refer to tests between experimental groups (details in the figure legend).

3 | RESULTS

3.1 | Rapid changes of astrocyte morphology after induction of epileptic activity

We first tested the hypothesis that induction of epileptiform activity induces rapid morphology changes of astrocytes. To this end, we visualized dye-filled astrocytes in the CA1 stratum radiatum of acute hippocampal slices by two-photon excitation fluorescence microscopy in parallel to electrophysiological recordings (Figure 1a). Astrocyte morphology changes were captured by measuring the fraction of tissue volume occupied by astrocyte processes within the territory of a single astrocyte (i.e., the astrocyte VF). This astrocyte VF is readily obtained by normalizing the average fluorescence intensity in a region of interest to that at the soma, because at the soma 100% of the tissue is occupied by the cell (Figure 1b). We have previously established that the astrocyte VF is a reliable and sensitive measure of astrocyte morphology, its fine details and its changes (Henneberger et al., 2020; Medvedev et al., 2014; Minge et al., 2021). Induction of epileptiform activity was achieved by bath application of penicillin, which disinhibits hippocampal networks by partial blockade of GABA_A receptors (Tsuda et al., 1994) (Suppl. Figure 1) and thereby reliably induces epileptiform activity in vitro and in vivo (Schwartzkroin & Prince, 1977). The extracellular K⁺ concentration (ACSF) was set to 5 mM (rats) or 4 mM (mice) throughout the entire experiments to obtain stable epileptiform discharges in hippocampal slices (Figure 1c, d). Tracking the VF of astrocytes filled with Texas red dextran (3 kDa) via the whole-cell patch pipette revealed a significant decrease of the astrocyte VF following the development of epileptiform activity (Figure 1e).

To test if this astrocyte morphology change also occurs in astrocytes that were not dialyzed by whole-cell patch clamp, we performed equivalent experiments in acute slices from mice expressing EGFP under a GFAP promoter in a subset of hippocampal astrocytes (Nolte et al., 2001). A similar and highly significant reduction of the astrocyte VF was observed (Figure 1f), which was not the result of a change of somatic EGFP fluorescence (somatic fluorescence relative to baseline, control $94.7 \pm 4.7\%$, penicillin $94.2 \pm 4.2\%$, $n = 14$ and 15 , $p > .15$ one-population t -tests, $p = .94$ two-population t -test). In a separate analysis of the same data, we quantified the area of the cross section of the astrocyte under investigation by drawing a polygonal region of interest around the astrocytes and measuring its area for the first and last recorded image. At the end of the control recording this area was $99.0 \pm 2.3\%$ relative to baseline ($n = 7$, $p = .69$, one population t -test) and $97.9 \pm 2.9\%$ in penicillin-treated slices ($n = 8$, $p = .47$, one population t -test) and no changes of the cross-section shape were observed. Thus, the boundary of astrocyte territories remained stable

while astrocytes occupied a reduced fraction of tissue volume within their territories. Importantly, this VF reduction was not observed when experiments were performed in the presence of channel and receptor blockers to inhibit action potential firing and glutamatergic synaptic transmission to suppress neuronal activity (Figure 1f, “Pen. in. inhib.”). This excludes the possibility that the VF reduction was caused by a direct and activity-independent effect of penicillin on astrocyte morphology. This conclusion is further supported by the observation of similar VF reductions in another in vitro model of epilepsy (wash-in of bicuculline and wash-out of Mg²⁺, Figure 1f). Therefore, induction of epileptiform activity in different experimental approaches and models leads to a robust and rapid reduction of the astrocyte VF.

We further tested if the astrocyte morphology change persisted beyond the induction of epileptiform activity. First, we monitored the astrocyte VF after washing out penicillin for another 40 min and detected no recovery of the VF (Figure 1g). Second, terminating epileptiform activity after 40 min by bath application of the sodium channel blocker TTX and recording the VF for further 40 min did not reveal a recovery either (Figure 1g). Taken together, induction of epileptiform activity induces a rapid astrocyte morphology change that persists at least 40 min beyond its induction. We further tested if astrocytes in the CA3 stratum radiatum show a similar morphological response to the induction of epileptiform activity. This was indeed the case (Figure 2a–d).

We next explored if such a rapid astrocyte morphology change is also triggered by epileptic activity in vivo. To this end, intracortical unilateral kainate/sham injections were performed in GFAP-EGFP mice ($n = 3$ for both groups), in which the success rate of inducing status epilepticus by kainate is $\sim 97\%$ (Bedner et al., 2015). Animals were sacrificed by perfusion fixation 30 min after kainate/sham injection, and hippocampal astrocyte morphology was analyzed. This revealed that astrocytes from kainate-injected animals had a significantly smaller VF than sham-injected animals (Figure 2e–g). Although transcardial perfusion with chemical fixatives has been shown to alter astrocyte morphology (Korogod et al., 2015), it is unlikely to have caused the observed differences: Both experimental groups were treated identically and VFs of astrocytes in the dentate gyrus measured in acute slices and by electron microscopy of chemically fixed tissue using the same technique as used here are an excellent match when tissue shrinkage is accounted for (Medvedev et al., 2014). Interestingly, an astrocyte VF reduction was also observed in the hippocampus contralateral to the kainate injection, indicating that spread of status-associated neuronal activity was sufficient to alter astrocyte morphology within 30 min. Together, these experiments reveal a yet unreported rapid morphological response of astrocytes to the induction of epileptiform and epileptic activity.

3.2 | Reduction of astrocyte intracellular diffusion and gap junction coupling

To further characterize the observed morphology change, we investigated if different parts of the astrocyte are selectively affected by the astrocyte VF reduction. Mapping the VF change onto the territory of



the astrocyte suggested that the morphology change occurred primarily in the periphery of the cells (Figure 3a). Correlating the initial VF with its change (Figure 3b) we found that the reduction was restricted to parts of the astrocytes where the initial VF was lower, that is, where medium-sized and small astrocytic processes populate the neuropil. We further characterized our findings by correlating local astrocyte VFs with the abundance of local GFAP. This was accomplished by correlating the local astrocyte VF in EGFP-expressing astrocytes and the corresponding local abundance of GFAP, which was labeled using immunohistochemistry (Figure 3c). As expected, we found that high local VF, that is, parts of the cells corresponding to large processes and the soma displayed high GFAP fluorescence intensities whereas areas with low local VFs were devoid of GFAP immunofluorescence (Figure 3d). Interestingly, the dependence of the GFAP intensity on the local VF overlapped with how the change of the astrocyte VF after induction of epileptiform depended on the initial VF (Figure 3b, d). In other words, the less GFAP is present in local astrocyte processes the more the local VF is reduced after induction of epileptiform activity.

Such a reduction of astrocytic cytosolic volume, which could reflect a withdrawal or shrinkage of small astrocytic processes, can be expected to affect diffusion inside the astrocyte. For instance, astrocyte process shrinkage could increase the tortuosity of the cytosolic space and thereby slow down diffusion processes, which can be quantified using FRAP of a cytosolic dye (Anders et al., 2014; Henneberger et al., 2020). We therefore measured FRAP of cytosolic EGFP before and after induction of epileptiform activity (Figure 4a, b). Indeed, FRAP was reduced after appearance of epileptiform activity but not in control recordings and FRAP relative to baseline was significantly lower in experiments where epileptiform activity had been induced compared to controls (Figure 4c–e). The emerging picture is thus that induction of epileptiform activity leads to a remodeling of peripheral astrocyte processes, which impairs diffusion in the cytosol of the astrocyte.

This decrease of intracellular diffusion could also reduce the diffusional coupling between astrocytes via gap junctions and thus signal exchange in the entire gap junction coupled astrocyte network. We have previously established the coupling length constant as a sensitive measure of astrocyte gap junction coupling (Anders et al., 2014) (Figure 5a, b). Measuring the coupling length constant after 20 min of dye loading into a single astrocyte and a second time after 30 more minutes of control recording or of induction of epileptiform activity revealed a significant reduction of dye coupling between astrocytes after induction of epileptiform activity (Figure 5c, d). This reduction of coupling was not the consequence of altered expression of connexin (Cx) 43 or 30 (Figure 5e, f). Also, analysis of the phosphorylation-dependent western blot bands (Deshpande et al., 2017; Solan & Lampe, 2009) did not reveal a detectable change of Cx43 phosphorylation patterns (Figure 5e, f). Because in the brain Cx43 is almost exclusively and Cx30 mostly expressed by astrocytes (He et al., 2018; Zhang et al., 2014) our results indicate that astrocyte Cx43/30 expression and Cx43 phosphorylation are not affected by induction of epileptiform activity. Therefore, the most parsimonious explanation

for the reduced astrocyte coupling is the reduction of intracellular diffusion. Taken together, the induction of epileptiform activity and the ensuing remodeling of peripheral astrocyte processes profoundly impairs diffusion within single astrocytes and, as a consequence, throughout astrocyte networks.

3.3 | Increase of epileptiform activity by ROCK-mediated astrocyte morphology changes

We next asked which astrocytic signaling molecules trigger the observed morphology changes. It is well established that GTPases of the Rho family and related pathways, for instance involving Rho-associated protein kinases (ROCK), control astrocyte morphology (for review see Zeug et al., 2018). Therefore, we tested if astrocyte morphology changes could be prevented by pharmacological inhibition of RhoA, Rac1, and ROCK. This was done by inducing epileptiform activity using penicillin in control recordings or in the presence of an inhibitor (Figure 6a). We found that inhibiting ROCK activity using Y-27632 prevented the astrocyte morphology change after induction of epileptiform activity (Figure 6a, b), which was not a result of Y-27632 affecting the action of penicillin on GABAergic synaptic transmission (Suppl. Figure 1). Similarly, in the presence of the RhoA inhibitor rhosin induction of epileptiform activity no longer affected astrocyte morphology, whereas the effect was preserved in experiments without an added drug and in the presence of the Rac1 inhibitor NSC 23766 (Figure 6b, time courses for rhosin and NSC not illustrated). In addition, we investigated a potential role of TNF- α signaling but found that acute bath application of TNF- α (10 ng/mL for 30 min) did not reduce the astrocytic VF compared to control recordings (TNF- α vs. control: $p = .44$ Student's t -test, $n = 10$ control and 9 for TNF- α). Furthermore, the effect of inducing epileptiform activity with penicillin on the astrocyte VF was preserved in TNF receptor 1 knockout mice (Peschon et al., 1998) (crossed with GFAP-EGFP mice; VF % of baseline: $78.9 \pm 3.70\%$, $n = 6$, $p = .0023$, Student's paired t -test vs. baseline). These results indicate that TNF- α signaling is unlikely to be involved in the rapid astrocyte morphology changes reported here, which, however, does not exclude other astrocyte-dependent roles of TNF- α signaling in epilepsy.

These results are in line with a RhoA-ROCK mediated astrocyte morphology change after induction of epileptiform activity. This is also plausible because a persistent increase of astrocytic RhoA activity leads to a astrocyte VF decrease (Domingos et al., 2023) that is similar to the one observed here after induction of epileptiform activity. However, pharmacological experiments cannot reveal if indeed astrocytic RhoA or ROCK is involved because they are expressed in many cell types. We therefore created conditional astrocytic knockout (aKO) lines of ROCK1 and ROCK2 (GLASTcreERT2 \times ROCK1^{loxP/loxP} \times flox-stop tdTomato, GLASTcreERT2 \times ROCK2^{loxP/loxP} \times flox-stop tdTomato) and a control mouse line (GLASTcreERT2 \times flox-stop tdTomato, see Material and Methods). All lines were injected with tamoxifen as described in Material and Methods to induce tdTomato expression, which was used for monitoring the VF in these experiments, and to

delete ROCK1 or 2 in the respective mouse lines. Before investigating astrocyte VF changes after induction of epileptiform activity, we characterized baseline astrocyte morphology and synaptic transmission in the CA1 stratum radiatum in acute slices from these mouse lines. We detected no differences in baseline astrocyte VF between control and ROCK1/2 aKO mice (VFs in %; control: 7.68 ± 0.87 , $n = 11$; ROCK1 aKO: 7.05 ± 0.57 , $n = 13$; ROCK2 aKO, $n = 15$: 7.36 ± 0.52 , one-way ANOVA $p = .81$). We also tested if field EPSPs (fEPSP) recorded from CA1 stratum radiatum in response to electrical stimulation of CA3-CA1 Schaffer collateral synapses were affected by aKO of ROCK1/2. We neither detected an effect on the fEPSP slope across a range of stimulation intensities (20, 30, ... 80 μ A; two-way repeated-measures ANOVA $p = .63$ for experimental group and $p < .001$ for stimulation intensity) nor did we observe differences between the fEPSP paired-pulse ratios as an indirect measure of the presynaptic release probability (interstimulus interval 50 ms, one-way ANOVA $p = .93$). Having established that aKO of ROCK1/2 does not alter the baseline astrocyte VF and basal functional parameters of synaptic transmission, we next tested if aKO of ROCK1/2 modifies the morphological response of astrocytes to the induction of epileptiform activity. We found that aKO of ROCK1 but not of ROCK2 prevented the astrocyte morphology change (Figure 6c, d). Analyzing the frequency of epileptiform discharge further revealed that aKO of ROCK1 but not of ROCK2 decreased the discharge rate (Figure 6e–g). Together these experiments demonstrate that astrocytic ROCK1 is required for the astrocyte morphology change following induction of epileptiform activity and that it increases the severity of epileptiform activity.

4 | DISCUSSION

Induction of epileptiform activity in vitro and status epilepticus in vivo rapidly changed hippocampal astrocyte morphology such that the fraction of tissue volume occupied by them was reduced within 30 min. This change occurred mostly at the level of small peripheral GFAP-negative branches. Whether this represents a first step of the more global morphological transformation seen later during epilepsy (see Introduction) or if these are independent phenomena is an interesting question for future studies. After induction in vitro, these morphology changes persisted even in the absence of network activity. Further analysis revealed that this astrocyte VF decrease occurred primarily at the level of small and medium sized astrocyte processes. Such a reduction of the local astrocyte volume could arise from a decrease of the size of astrocyte processes or their number or both in a given tissue volume (Minge et al., 2021). Because astrocyte processes can be as thin as 50–100 nm they cannot be fully resolved using the diffraction limited multiphoton microscopy used here (Heller & Rusakov, 2017). Therefore, for a full characterization of rapid epilepsy-related astrocyte morphology further experiments using techniques with higher spatial resolution will be required, for example expansion microscopy (Brunskine et al., 2022; Chen et al., 2015; Herde et al., 2020). However, our current experiments already provide some clues of what to expect. FRAP experiments revealed that the diffusion in the astrocyte cytosol is slowed down after induction of epileptiform

activity. For simplicity, we could consider the astrocyte cytosol to be a porous medium like the extracellular space (ECS) with a VF and a tortuosity. The effective diffusion coefficient of a molecule in the ECS decreases when the ECS tortuosity increases (Nicholson, 2001). This indicates that the tortuosity of the astrocyte cytosol has increased after induction of epileptiform activity. Over certain ranges, tortuosity and VF are roughly inversely related in the ECS (Krizaj et al., 1996; Kume-Kick et al., 2002) suggesting that the observed astrocyte VF reduction is sufficient for explaining the decreased intracellular diffusion. We further observed reduced dye-coupling in the astrocyte network without detectable changes of Cx43/Cx30 expression and Cx43 phosphorylation. This suggests that the decreased dye coupling, that is, the decreased intercellular diffusion in the astrocyte network, is a consequence of the astrocyte morphology changes. This could represent a first step towards the uncoupling of astrocyte networks in epilepsy models and human temporal lobe epilepsy (Bedner et al., 2015).

To our knowledge, the astrocyte morphology changes detected here occur much earlier than what was previously described in CA1 stratum radiatum. For instance, a shortening of GFAP-positive larger processes has been reported to occur within 4 h after induction of status epilepticus (Henning, Antony, et al., 2023) whereas kindling induced by electrical stimulation led to an increase of the astrocyte VF within 24–48 h (Hawrylak et al., 1993). It was also shown that induction of focal epileptiform activity and kainate injections alter the morphology of GFAP-positive and perisynaptic processes within a week (Clarkson et al., 2020; Oberheim et al., 2008; Takahashi et al., 2010). Another example is the effect of status epilepticus in the lithium-pilocarpine model on astrocyte morphology after 2–4 weeks (Plata et al., 2018). Together, these studies and the present results indicate that astrocyte morphology is continuously changing starting almost immediately after the initial epileptogenic trigger. In contrast, the type of astrocyte morphology changes that were observed on the level of small and medium-sized astrocyte processes varies between studies. In human tissue samples from patients with temporal lobe epilepsy, astrocytes occupied a higher fraction of tissue volume in severe cases when compared to mild cases and astrocytic processes approached excitatory synapses less often in severe cases compared to mild cases (Witcher et al., 2010). An increased astrocytic VF was also observed 24–48 h after kindling (Hawrylak et al., 1993). In addition, astrocytic processes enwrapped excitatory synapses more strongly 1 week after kainate-induced status epilepticus (Clarkson et al., 2020). 2–4 weeks after induction of status epilepticus, the number of distal astrocyte processes was reduced but the VF of small processes (not resolvable by diffraction-limited microscopy) was unaffected (Plata et al., 2018). Because of the different epilepsy models, technical approaches and analyzed morphological parameters it is currently difficult to reconstruct a detailed timeline of progressive astrocyte morphology changes. This is also a complex issue because neuronal changes such as neuronal death and synapse loss are likely progressing too (Clarkson et al., 2020; Hawrylak et al., 1993; Witcher et al., 2010), which complicates the comparison of analyses focusing on synapses (e.g., astrocyte synapse enwrapping) and those quantifying other morphological features.

4.1 | Molecular signals driving astrocyte morphology changes

Our experiments reveal that astrocyte morphology changes after induction of epileptiform activity *in vitro* can be prevented by inhibiting RhoA and ROCK and by conditionally deleting the ROCK isoform ROCK1 in astrocytes (but not ROCK2). Both RhoA and ROCK are well known to control the astrocyte cytoskeleton and astrocyte morphology (for review see Zeug et al., 2018). This is also consistent with our recent work indicating that RhoA is a powerful regulator of hippocampal astrocyte morphology, which decreases the astrocyte VF on the level of small peripheral astrocyte processes when overexpressed (Domingos et al., 2023). We have also previously shown that inhibiting cofilin phosphorylation by LIMK, a target of ROCK, prevents an astrocyte process withdrawal from excitatory synapse triggered by the induction of long-term potentiation of synaptic transmission (Henneberger et al., 2020), which was also reflected by a decrease of the astrocyte VF. For these reasons, it is likely that the onset of epileptiform activity increases astrocytic RhoA and ROCK1 activity and thereby modifies the astrocyte cytoskeleton and morphology.

How RhoA activity is increased in our experiments remains to be established. It has previously been shown that eliciting epileptiform activity in hippocampal slices induces Ca^{2+} signals in astrocytes (Fellin et al., 2006; Tian et al., 2005). However, increasing astrocytic Ca^{2+} signaling alone by various stimuli did not reproduce the astrocyte VF reduction after synaptic long-term potentiation (Henneberger et al., 2020). Instead, inhibition of NKCC1 prevented this reduction, which implies that NKCC1 could control the activity of astrocytic RhoA/ROCK1. There is indeed accumulating evidence from other cell types that NKCC1 can control the activity of RhoA and Rac1 (Ma et al., 2019; Schiapparelli et al., 2017). Additionally, the transport rate of NKCC1 in astrocytes is increased when extracellular K^+ is elevated (Su et al., 2002), which is likely to be the case during epileptiform activity. A likely scenario is therefore that the increased neuronal activity after induction of epileptiform activity initiates an astrocyte morphology change via NKCC1, and in turn activation of RhoA and ROCK1. However, a direct link between NKCC1 activity and RhoA in astrocytes remains to be demonstrated. In addition to such a role in cytoskeletal remodeling, astrocytic NKCC1 regulates astrocytic chloride homeostasis (Engels et al., 2021) and has been shown to inhibit seizure-like events induced by tetanic stimulation in the hippocampus (Nguyen et al., 2023). Astrocytic NKCC1 could therefore have multiple and potentially opposing roles in epilepsy.

4.2 | Interdependence of morphology changes and epileptic activity

One could speculate that the observed astrocyte morphology changes support the development of epileptiform activity and potentially of epilepsy because the morphology changes develop in parallel to epileptiform activity. This hypothesis is also supported by the fact that astrocytic ROCK1 deletion prevents not only the morphology but also reduces epileptiform activity. This scenario is intriguing because the

morphology changes persist beyond their induction, also in the absence of neuronal activity. This could lock the hippocampus in a state of increased excitability if rapid astrocyte morphology changes had indeed a supportive role for epileptic activity. However, ROCK signaling can have many targets in addition to cytoskeleton-related factors (Amano et al., 2010; Riento & Ridley, 2003). The alternative is therefore that astrocytic ROCK1 signaling modifies astrocyte morphology and also an additional astrocyte mechanism in parallel, which is responsible for increasing epileptiform activity.

Assuming that the rapid astrocyte morphology change indeed supports epileptiform activity, what would be candidate mechanisms? Small and medium-sized astrocyte processes are ideally positioned in the neuropil and near synapses to fulfill their many known functions (e.g., neurotransmitter clearance, maintaining ion homeostasis, modulation of synapse function by gliotransmission). A remodeling of these astrocyte processes is going to affect their spatial relationship with synapses and other neuronal compartments and could thereby alter all mechanisms that depend on proximity (e.g., efficiency of neurotransmitter uptake or gliotransmission). Among the many candidate mechanisms, glutamate and potassium uptake have been directly linked to the astrocyte changes that we have observed here.

The question whether a change of astrocyte potassium buffering affects epileptogenesis and epilepsy has been intensely investigated, as recently reviewed by (Henning, Unichenko, et al., 2023). A direct link between our experimental results and previous studies is the acute reduction of gap junction coupling between astrocytes. It was for instance found that a reduction of astrocyte coupling to half of control values 4 h after kainate-induced status epilepticus prevented the effect of pharmacological gap junction blockade on an indirect measure of extracellular potassium transients (Bedner et al., 2015). In contrast, a similar reduction of astrocyte coupling did not significantly affect potassium transients recorded from astrocytes in acute slices two to four weeks after induction of status epilepticus in the lithium-pilocarpine model (Plata et al., 2018), which may be explained by long-term adaptive changes of potassium clearance. In our experiments, we detected a ~20% reduction of the coupling strength over 30 min. Considering that the near-complete acute block of gap junctions increases locally induced potassium transients by ~30% only if their amplitude is higher than ~10 mM (Breithausen et al., 2020), it seems unlikely that the observed much smaller reduction of astrocyte coupling has a significant impact on potassium clearance in acute slices. Indeed, we could confirm that induction of epileptiform activity by penicillin does not affect K^+ -transients induced by later synaptic stimulation (Suppl. Figure 2). However, it is worth noting that this does not rule out stronger uncoupling, as observed *in vivo* and/or later time points (see for instance Bedner et al., 2015), perturbs potassium homeostasis during an epileptic seizure.

Similar to potassium buffering, the role of altered astrocytic glutamate uptake in epilepsy has been explored in detail, for review see (Peterson & Binder, 2020). Regarding the link between astrocyte morphology changes and glutamate uptake, it was found that glutamate clearance was accelerated while astrocytic coverage was increased at the synapses remaining 1–2 weeks after induction of status

epilepticus using kainate (Clarkson et al., 2020; Takahashi et al., 2010). Such a relationship between the glutamate clearance and perisynaptic presence of astrocyte processes has also been found under physiological conditions. For instance, the coverage of dendritic spines by astrocytic glutamate transporters relative to the spine size determines the efficiency of local glutamate uptake (Herde et al., 2020). Also the induction of synaptic long-term potentiation leads to a withdrawal of perisynaptic astrocytic processes and increased diffusion of synaptically released glutamate into extrasynaptic space and increased synaptic crosstalk (Henneberger et al., 2020). In addition, retraction of perisynaptic astrocyte processes by decreasing the astrocytic expression of ezrin increases glutamate crosstalk (Badia-Soteras et al., 2022). If the astrocyte morphology changes observed here indeed represent a withdrawal of astrocyte processes from excitatory synapses, a reduced glutamate uptake could explain how astrocytic ROCK-signaling and morphology changes support epileptiform activity. However, as pointed out above, it remains to be established how precisely the induction of epileptiform activity changes the spatial relationship between astrocyte processes and glutamatergic synapses and also GABAergic contacts (Brunskine et al., 2022; Herde et al., 2020).

5 | CONCLUSION

Together our results reveal that astrocytic ROCK1 signaling mediates a rapid astrocyte morphology change after the onset of epileptiform activity in vitro, which is also observed after status epilepticus in vivo. The signaling pathways and the morphology change are similar to those triggered in physiological experiments and inhibiting these pathways also reduces epileptiform activity in vitro. Together this suggests that the described morphology change is a maladaptive morphological response by astrocytes in the context of epilepsy.

This emphasizes that Rho/ROCK and related signaling pathways are interesting targets for modulating epilepsy (İnan & Büyükaşar, 2008; Kourdougli et al., 2015; Zhang et al., 2015). Although pharmacological inhibition of ROCK using i.p. injections, which are neither selective for the brain nor for astrocytes, had inconsistent outcomes in epilepsy models (İnan & Büyükaşar, 2008; Kourdougli et al., 2015), testing the effect of astrocyte specific manipulations of RhoA/ROCK signaling in vivo in suitable epilepsy models appears to be promising.

AUTHOR CONTRIBUTIONS

Stefanie Anders, Björn Breithausen, Petr Unichenko, Michel K. Herde, Daniel Minge, Charlotte Behringer, Adlin Abramian, Cátia Domingos, and Christian Henneberger performed and analyzed electrophysiological and imaging experiments in acute slices. In vivo epilepsy experiments and their analysis was done by Peter Bedner, Michel K. Herde, Lukas Henning, Julika Pitsch, and Christian Henneberger. Tushar Deshpande did western blot experiments and analyzed them. Björn Breithausen and Anne Boehlen performed additional electrophysiological tests. Young-Bum Kim provided the LoxP-flanked ROCK1 mice used in the study. Christian

Steinhäuser provided materials such as the custom-made Cx43 antibody and designed and supervised kainate-injection experiments. Christian Henneberger conceived the study and wrote the initial version of the manuscript, to which all authors subsequently contributed.

ACKNOWLEDGMENTS

We thank Gerald Seifert and Thomas Erdmann for support with animal breeding and genotyping. The study was supported by the NRW-Rückkehrerprogramm, the Human Frontiers Science Program, German Research Foundation (DFG, SFB1089 and SPP1757), the National Institutes of Health (NIH, R01DK129946 to Young-Bum Kim). Open Access funding enabled and organized by Projekt DEAL.

DATA AVAILABILITY STATEMENT

The data that support the findings of this study are available from the corresponding author upon reasonable request.

ORCID

Peter Bedner  <https://orcid.org/0000-0003-0090-7553>

Christian Steinhäuser  <https://orcid.org/0000-0003-2579-8357>

Christian Henneberger  <https://orcid.org/0000-0002-5391-7387>

REFERENCES

- Amano, M., Tsumura, Y., Taki, K., Harada, H., Mori, K., Nishioka, T., Kato, K., Suzuki, T., Nishioka, Y., Iwamatsu, A., & Kaibuchi, K. (2010). A proteomic approach for comprehensively screening substrates of protein kinases such as rho-kinase. *PLoS One*, 5, e8704.
- Anders, S., Minge, D., Griemsmann, S., Herde, M. K., Steinhäuser, C., & Henneberger, C. (2014). Spatial properties of astrocyte gap junction coupling in the rat hippocampus. *Philosophical Transactions of the Royal Society B*, 369, 20130600.
- Badia-Soteras, A., Heistek, T. S., Kater, M. S. J., Mak, A., Negrean, A., van den Oever, M. C., Mansvelder, H. D., Khakh, B. S., Min, R., Smit, A. B., & Verheijen, M. H. G. (2022). Retraction of astrocyte leaflets from the synapse enhances fear memory. *Biological Psychiatry*, 94, 226–238.
- Bedner, P., Dupper, A., Hüttmann, K., Müller, J., Herde, M. K., Dublin, P., Deshpande, T., Schramm, J., Häussler, U., Haas, C. A., Henneberger, C., Theis, M., & Steinhäuser, C. (2015). Astrocyte uncoupling as a cause of human temporal lobe epilepsy. *Brain*, 138, 1208–1222.
- Bernardinelli, Y., Randall, J., Janett, E., Nikonenko, I., König, S., Jones, E. V., Flores, C. E., Murai, K. K., Bochet, C. G., Holtmaat, A., & Muller, D. (2014). Activity-dependent structural plasticity of Perisynaptic astrocytic domains promotes excitatory synapse stability. *Current Biology*, 24, 1679–1688.
- Bordey, A., & Sontheimer, H. (1998). Properties of human glial cells associated with epileptic seizure foci. *Epilepsy Research*, 32, 286–303.
- Breithausen, B., Kautzmann, S., Boehlen, A., Steinhäuser, C., & Henneberger, C. (2020). Limited contribution of astroglial gap junction coupling to buffering of extracellular K⁺ in CA1 stratum radiatum. *Glia*, 68, 918–931.
- Brunskine, C., Passlick, S., & Henneberger, C. (2022). Structural heterogeneity of the GABAergic tripartite synapse. *Cell*, 11, 3150.
- Chen, F., Tillberg, P. W., & Boyden, E. S. (2015). Expansion microscopy. *Science*, 347, 543–548.
- Clarkson, C., Smeal, R. M., Hasenoehrl, M. G., White, J. A., Rubio, M. E., & Wilcox, K. S. (2020). Ultrastructural and functional changes at the tripartite synapse during epileptogenesis in a model of temporal lobe epilepsy. *Experimental Neurology*, 326, 113196.



- Deshpande, T., Li, T., Herde, M. K., Becker, A., Vatter, H., Schwarz, M. K., Henneberger, C., Steinhäuser, C., & Bedner, P. (2017). Subcellular reorganization and altered phosphorylation of the astrocytic gap junction protein connexin43 in human and experimental temporal lobe epilepsy. *Glia*, 65, 1809–1820.
- Domingos, C., Müller, F. E., Passlick, S., Wachten, D., Ponimaskin, E., Schwarz, M. K., Schoch, S., Zeug, A., & Henneberger, C. (2023). Induced remodelling of astrocytes in vitro and in vivo by manipulation of astrocytic RhoA activity. *Cell*, 12, 331.
- Engels, M., Kalia, M., Rahmati, S., Petersilie, L., Kovermann, P., van Putten, M. J. A. M., Rose, C. R., Meijer, H. G. E., Gensch, T., & Fahlke, C. (2021). Glial chloride homeostasis under transient ischemic stress. *Frontiers in Cellular Neuroscience*, 15, 735300. <https://doi.org/10.3389/fncel.2021.735300>
- Escartin, C., Galea, E., Lakatos, A., O'Callaghan, J. P., Petzold, G. C., Serrano-Pozo, A., Steinhäuser, C., Volterra, A., Carmignoto, G., Agarwal, A., Allen, N. J., Araque, A., Barbeito, L., Barzilai, A., Bergles, D. E., Bonvento, G., Butt, A. M., Chen, W.-T., Cohen-Salmon, M., ... Verkhratsky, A. (2021). Reactive astrocyte nomenclature, definitions, and future directions. *Nature Neuroscience*, 24, 312–325.
- Fellin, T., Gomez-Gonzalo, M., Gobbo, S., Carmignoto, G., & Haydon, P. G. (2006). Astrocytic glutamate is not necessary for the generation of epileptiform neuronal activity in hippocampal slices. *The Journal of Neuroscience*, 26, 9312–9322.
- Haber, M., Zhou, L., & Murai, K. K. (2006). Cooperative astrocyte and dendritic spine dynamics at hippocampal excitatory synapses. *The Journal of Neuroscience*, 26, 8881–8891.
- Hawrylak, N., Chang, F. L., & Greenough, W. T. (1993). Astrocytic and synaptic response to kindling in hippocampal subfield CA1. II. Synaptogenesis and astrocytic process increases in vivo kindling. *Brain Research*, 603, 309–316.
- He, L., Vanlandewijck, M., Mäe, M. A., Andrae, J., Ando, K., Del Gaudio, F., Nahar, K., Lebouvier, T., Laviña, B., Gouveia, L., Sun, Y., Raschperger, E., Segerstolpe, Å., Liu, J., Gustafsson, L., Räsänen, M., Zarb, Y., Mochizuki, N., Keller, A., ... Betsholtz, C. (2018). Single-cell RNA sequencing of mouse brain and lung vascular and vessel-associated cell types. *Scientific Data*, 5, 180160.
- Heller, J. P., & Rusakov, D. A. (2017). The nanoworld of the tripartite synapse: Insights from super-resolution microscopy. *Frontiers in Cellular Neuroscience*, 11, 374.
- Henneberger, C., Bard, L., Panatier, A., Reynolds, J. P., Kopach, O., Medvedev, N. I., Minge, D., Herde, M. K., Anders, S., Kraev, I., Heller, J. P., Rama, S., Zheng, K., Jensen, T. P., Sanchez-Romero, I., Jackson, C. J., Janovjak, H., Ottersen, O. P., Nagelhus, E. A., ... Rusakov, D. A. (2020). LTP induction boosts glutamate spillover by driving withdrawal of perisynaptic astroglia. *Neuron*, 108, 919–936.e11.
- Henneberger, C., & Rusakov, D. A. (2012). Monitoring local synaptic activity with astrocytic patch pipettes. *Nature Protocols*, 7, 2171–2179.
- Henning, L., Antony, H., Breuer, A., Müller, J., Seifert, G., Audinat, E., Singh, P., Brosse, F., Heneka, M. T., Steinhäuser, C., & Bedner, P. (2023). Reactive microglia are the major source of tumor necrosis factor alpha and contribute to astrocyte dysfunction and acute seizures in experimental temporal lobe epilepsy. *Glia*, 71, 168–186.
- Henning, L., Unichenko, P., Bedner, P., Steinhäuser, C., & Henneberger, C. (2023). Overview article astrocytes as initiators of epilepsy. *Neurochemical Research*, 48, 1091–1099.
- Herde, M. K., Bohmbach, K., Domingos, C., Vana, N., Komorowska-Müller, J. A., Passlick, S., Schwarz, I., Jackson, C. J., Dietrich, D., Schwarz, M. K., & Henneberger, C. (2020). Local efficacy of glutamate uptake decreases with synapse size. *Cell Reports*, 32, 108182.
- Hirrlinger, J., Hülsmann, S., & Kirchhoff, F. (2004). Astroglial processes show spontaneous motility at active synaptic terminals in situ. *The European Journal of Neuroscience*, 20, 2235–2239.
- Huang, H., Kong, D., Byun, K. H., Ye, C., Koda, S., Lee, D. H., Oh, B.-C., Lee, S. W., Lee, B., Zabolotny, J. M., Kim, M. S., Bjørnbæk, C., Lowell, B. B., & Kim, Y.-B. (2012). Rho-kinase regulates energy balance by targeting hypothalamic leptin receptor signaling. *Nature Neuroscience*, 15, 1391–1398.
- Inan, S. Y., & Büyükaşar, K. (2008). Antiepileptic effects of two rho-kinase inhibitors, Y-27632 and fasudil, in mice. *British Journal of Pharmacology*, 155, 44–51.
- Korogod, N., Petersen, C. C., & Knott, G. W. (2015). Ultrastructural analysis of adult mouse neocortex comparing aldehyde perfusion with cryo fixation. *eLife*, 4, e05793.
- Kourdougli, N., Varpula, S., Chazal, G., & Rivera, C. (2015). Detrimental effect of post status epilepticus treatment with ROCK inhibitor Y-27632 in a pilocarpine model of temporal lobe epilepsy. *Frontiers in Cellular Neuroscience*, 9, 413.
- Krizaj, D., Rice, M. E., Wardle, R. A., & Nicholson, C. (1996). Water compartmentalization and extracellular tortuosity after osmotic changes in cerebellum of *Trachemys scripta*. *The Journal of Physiology*, 492, 887–896.
- Kume-Kick, J., Mazel, T., Voříšek, I., Hrabětová, S., Tao, L., & Nicholson, C. (2002). Independence of extracellular tortuosity and volume fraction during osmotic challenge in rat neocortex. *The Journal of Physiology*, 542, 515–527.
- Kümper, S., Mardakheh, F. K., McCarthy, A., Yeo, M., Stamp, G. W., Paul, A., Worboys, J., Sadok, A., Jørgensen, C., Guichard, S., & Marshall, C. J. (2016). Rho-associated kinase (ROCK) function is essential for cell cycle progression, senescence and tumorigenesis. *eLife*, 5, e12203.
- Lushnikova, I., Skibo, G., Muller, D., & Nikonenko, I. (2009). Synaptic potentiation induces increased glial coverage of excitatory synapses in CA1 hippocampus. *Hippocampus*, 19, 753–762.
- Ma, H., Li, T., Tao, Z., Hai, L., Tong, L., Yi, L., Abeysekera, I. R., Liu, P., Xie, Y., Li, J., Yuan, F., Zhang, C., Yang, Y., Ming, H., Yu, S., & Yang, X. (2019). NKCC1 promotes EMT-like process in GBM via RhoA and Rac1 signaling pathways. *Journal of Cellular Physiology*, 234, 1630–1642.
- Madisen, L., Zwingman, T. A., Sunken, S. M., Oh, S. W., Zariwala, H. A., Gu, H., Ng, L. L., Palmiter, R. D., Hawrylycz, M. J., Jones, A. R., Lein, E. S., & Zeng, H. (2010). A robust and high-throughput Cre reporting and characterization system for the whole mouse brain. *Nature Neuroscience*, 13, 133–140.
- Medvedev, N., Popov, V., Henneberger, C., Kraev, I., Rusakov, D. A., & Stewart, M. G. (2014). Glia selectively approach synapses on thin dendritic spines. *Philosophical Transactions of the Royal Society B*, 369, 20140047.
- Minge, D., Domingos, C., Unichenko, P., Behringer, C., Pauletti, A., Anders, S., Herde, M. K., Delekate, A., Gulakova, P., Schoch, S., Petzold, G. C., & Henneberger, C. (2021). Heterogeneity and development of fine astrocyte morphology captured by diffraction-limited microscopy. *Frontiers in Cellular Neuroscience*, 15, 669280.
- Mori, T., Tanaka, K., Buffo, A., Wurst, W., Kühn, R., & Götz, M. (2006). Inducible gene deletion in astroglia and radial glia—A valuable tool for functional and lineage analysis. *Glia*, 54, 21–34.
- Nguyen, T. D., Ishibashi, M., Sinha, A. S., Watanabe, M., Kato, D., Horiuchi, H., Wake, H., & Fukuda, A. (2023). Astrocytic NKCC1 inhibits seizures by buffering Cl[−] and antagonizing neuronal NKCC1 at GABAergic synapses. *Epilepsia*. <https://doi.org/10.1111/epi.17784>
- Nicholson, C. (2001). Diffusion and related transport mechanisms in brain tissue. *Reports on Progress in Physics*, 64, 815–884.
- Niquet, J., Ben-Ari, Y., & Represa, A. (1994). Glial reaction after seizure induced hippocampal lesion: Immunohistochemical characterization of proliferating glial cells. *Journal of Neurocytology*, 23, 641–656.
- Nolte, C., Matyash, M., Pivneva, T., Schipke, C. G., Ohlemeyer, C., Hanisch, U., Kirchhoff, F., & Kettenmann, H. (2001). GFAP promoter-controlled EGFP-expressing transgenic mice: A tool to visualize astrocytes and astrogliosis in living brain tissue. *Glia*, 33, 72–86.

- Oberheim, N. A., Tian, G.-F., Han, X., Peng, W., Takano, T., Ransom, B., & Nedergaard, M. (2008). Loss of astrocytic domain organization in the epileptic brain. *The Journal of Neuroscience*, 28, 3264–3276.
- Ortinski, P. I., Dong, J., Mungenast, A., Yue, C., Takano, H., Watson, D. J., Haydon, P. G., & Coulter, D. A. (2010). Selective induction of astrocytic gliosis generates deficits in neuronal inhibition. *Nature Neuroscience*, 13, 584–591.
- Pekny, M., & Pekna, M. (2014). Astrocyte reactivity and reactive astrogliosis: Costs and benefits. *Physics Review*, 94, 1077–1098.
- Peschon, J. J., Torrance, D. S., Stocking, K. L., Glaccum, M. B., Otten, C., Willis, C. R., Charrier, K., Morrissey, P. J., Ware, C. B., & Mohler, K. M. (1998). TNF receptor-deficient mice reveal divergent roles for p55 and p75 in several models of inflammation. *Journal of Immunology*, 160, 943–952.
- Peterson, A. R., & Binder, D. K. (2020). Astrocyte glutamate uptake and signaling as novel targets for antiepileptogenic therapy. *Frontiers in Neurology*, 11, 1006.
- Plata, A., Lebedeva, A., Denisov, P., Nosova, O., Postnikova, T. Y., Pimashkin, A., Brazhe, A., Zaitsev, A. V., Rusakov, D. A., & Semyanov, A. (2018). Astrocytic atrophy following status epilepticus parallels reduced Ca²⁺ activity and impaired synaptic plasticity in the rat hippocampus. *Frontiers in Molecular Neuroscience*, 11, 215.
- Riento, K., & Ridley, A. J. (2003). ROCKs: Multifunctional kinases in cell behaviour. *Nature Reviews. Molecular Cell Biology*, 4, 446–456.
- Robel, S., Buckingham, S. C., Boni, J. L., Campbell, S. L., Danbolt, N. C., Riedemann, T., Sutor, B., & Sontheimer, H. (2015). Reactive astrogliosis causes the development of spontaneous seizures. *The Journal of Neuroscience*, 35, 3330–3345.
- Schiapparelli, P., Guerrero-Cazares, H., Magaña-Maldonado, R., Hamilla, S. M., Ganaha, S., Goulin Lippi Fernandes, E., Huang, C.-H., Aranda-Espinoza, H., Devreotes, P., & Quinones-Hinojosa, A. (2017). NKCC1 regulates migration ability of glioblastoma cells by modulation of actin dynamics and interacting with cofilin. *eBioMedicine*, 21, 94–103.
- Schwartzkroin, P. A., & Prince, D. A. (1977). Penicillin-induced epileptiform activity in the hippocampal in vitro preparation. *Annals of Neurology*, 1, 463–469.
- Solan, J. L., & Lampe, P. D. (2009). Connexin43 phosphorylation: Structural changes and biological effects. *The Biochemical Journal*, 419, 261–272.
- Su, G., Kintner, D. B., Flagella, M., Shull, G. E., & Sun, D. (2002). Astrocytes from Na⁺-K⁺-Cl⁻ cotransporter-null mice exhibit absence of swelling and decrease in EAA release. *American Journal of Physiology-Cell Physiology*, 282, C1147–C1160.
- Takahashi, D. K., Vargas, J. R., & Wilcox, K. S. (2010). Increased coupling and altered glutamate transport currents in astrocytes following kainic-acid-induced status epilepticus. *Neurobiology of Disease*, 40, 573–585.
- Tian, G.-F., Azmi, H., Takano, T., Xu, Q., Peng, W., Lin, J., Oberheim, N., Lou, N., Wang, X., Zielke, H. R., Kang, J., & Nedergaard, M. (2005). An astrocytic basis of epilepsy. *Nature Medicine*, 11, 973–981.
- Tsuda, A., Ito, M., Kishi, K., Shiraishi, H., Tsuda, H., & Mori, C. (1994). Effect of penicillin on GABA-gated chloride ion influx. *Neurochemical Research*, 19, 1–4.
- Witcher, M. R., Park, Y. D., Lee, M. R., Sharma, S., Harris, K. M., & Kirov, S. A. (2010). Three-dimensional relationships between perisynaptic astroglia and human hippocampal synapses. *Glia*, 58, 572–587.
- Zeug, A., Müller, F. E., Anders, S., Herde, M. K., Minge, D., Ponimaskin, E., & Henneberger, C. (2018). Control of astrocyte morphology by rho GTPases. *Brain Research Bulletin*, 136, 44–53.
- Zhang, Y., Chen, K., Sloan, S. A., Bennett, M. L., Scholze, A. R., O'Keeffe, S., Phatnani, H. P., Guarnieri, P., Caneda, C., Ruderisch, N., Deng, S., Liddel, S. A., Zhang, C., Daneman, R., Maniatis, T., Barres, B. A., & Wu, J. Q. (2014). An RNA-sequencing transcriptome and splicing database of glia, neurons, and vascular cells of the cerebral cortex. *The Journal of Neuroscience*, 34, 11929–11947.
- Zhang, Y., Liu, J., Luan, G., & Wang, X. (2015). Inhibition of the small GTPase Cdc42 in regulation of epileptic-seizure in rats. *Neuroscience*, 289, 381–391.

SUPPORTING INFORMATION

Additional supporting information can be found online in the Supporting Information section at the end of this article.

How to cite this article: Anders, S., Breithausen, B., Unichenko, P., Herde, M. K., Minge, D., Abramian, A., Behringer, C., Deshpande, T., Boehlen, A., Domingos, C., Henning, L., Pitsch, J., Kim, Y.-B., Bedner, P., Steinhäuser, C., & Henneberger, C. (2024). Epileptic activity triggers rapid ROCK1-dependent astrocyte morphology changes. *Glia*, 72(3), 643–659. <https://doi.org/10.1002/glia.24495>